J. of Biomechanics, 40(4):851-860, 2007

In Vivo Biomechanics of the Fingerpad Skin Under Local Tangential Traction

Qi Wang and Vincent Hayward *

Haptics Laboratory, Centre for Intelligent Machines, McGill University, 3480 University Street, Montréal, H3A 2A7, Canada

Abstract

Small patches of fingerpad glabrous skin in human subjects were tested in vivo for their biomechanical properties under tangential loading and for large deformations. These conditions included stretching and shearing the skin at a length scale of 0.3 mm using an apparatus comprising a pair of piezoelectric benders arranged to increase the stiffness/free deflection tradeoff when compared to ordinary cantilevered benders. It was then possible to test the skin with up to 80% of tangential strain. With feedback control, it was also possible to create isotonic and isometric testing conditions. The results showed much variability across subjects and it was seen that the glabrous skin exhibited nonlinear stiffening in tangential traction. The skin was consistently more elastic across the ridges than along the ridges regardless of the location of the sample on the fingerpad. The skin behaved visco-elastically but relaxed about twice as fast than it crept. Finally, it was found that under large deformation, there was consistently an 80% of hysteretic loss for a wide range of loading conditions.

Key words: Fingerpad skin properties; In vivo tissue measurement; Biomechanics; Fingers.
Word count (main text): 3500.

* Corresponding author. Centre for Intelligent Machines, McGill University, 3480 University Street, Montréal, H3A 2A7, Canada. Tel. +1-514-398-5006, Fax. +1-514-398-7348.
Email address: hayward@cim.mcgill.ca (Vincent Hayward).

1 Introduction

An important function of the glabrous skin is to mediate tactile sensations. When the skin comes in contact with an object, mechanical loading causes it to deform from a relaxed state. Several types of mechanoreceptors signal these deformations to the central nervous system (CNS), ultimately resulting in the perception of the object's attributes such as shape or compliance. Many studies have attempted to identify the responses of these cutaneous receptors under various loads (Johansson and Vallbo, 1979b; Phillips and Johnson, 1981a; Johansson and Vallbo, 1983; Johansson and Westling, 1984, 1987; Srinivasan and LaMotte, 1987; Johnson and Hsiao, 1992; Edin and Johansson, 1995; Goodwin et al., 1997; Bisley et al., 2000; Johnson, 2001; Johansson and Birznieks, 2004). It would seem that a characterization of the biomechanics of the glabrous skin would contribute to the understanding of the tactile function since receptors respond to patterns of skin deformation (Goodwin and Wheat, 2004). Birznieks et al. (2001) suggested that different strain patterns caused by anisotropic material properties might account for the directionality of tactile afferent responses. Moy et al. (2000a) found that viscoelasticity had significant effect on tactile perception. Biggs and Srinivasan (2002) reported that some individuals were more sensitive to tangential forces than to normal forces on their forearms, but the opposite was true on their fingerpads. Taken together, these observations suggest that the biomechanics of the skin could have functional consequences for how mechanoreceptors in the skin are stimulated and for the type of signals sent to the brain.

Cauna (1954) argued with the aid of an analog model that the structure of papillary ridges acted as "a magnifying lever mechanism for transmission of touch stimuli to the underlying receptors". Since then, there has been much interest in numerical models to elucidate the function of receptors embedded in the skin (Phillips and Johnson, 1981b; Srinivasan and Dandekar, 1996; Maeno et al., 1998; Moy et al., 2000a; Wu et al., 2003b; Gerling and Thomas, 2005). Lack of knowledge of the glabrous skin's properties led some authors to use numbers measured for the hairy skin. Others solved an inverse problem by matching the predicted shape with measurements, but the results were unreliable because of the assumptions required. Knowledge of the detailed behavior of the skin could also be of interest to tactile display designers (Moy et al., 2000b; Drewing et al., 2005; Levesque et al., 2005), and have numerous clinical applications (Payne, 1991).

During the course of daily handling of objects and exploratory touching, the fingerpad can experience considerable global deformation. For instance, 0.75 N of force could cause about 1.5 mm of normal deformation of a fingertip tapping at 0.5 Hz (Serina et al., 1997); 1.9 N of shearing force can induce about 4 mm of tangential deformation (Nakazawa et al., 2000). The global viscoelastic behavior of the fingerpad, thought to be important in the manipulative tasks, was the subject of several studies (Serina et al., 1997, 1998; Pawluk and Howe, 1999; Wu et al., 2003a,b; Jindrich et al., 2003; Pataky et al., 2005), but locally, the fingerpad skin also experiences considerable deformation: the act of sliding the fingertip on a flat glass surface can result in local tangential deformation of $\pm$ 30 % (Levesque and Hayward, 2003). The viscoelasticity of human hairy skin has been demonstrated in vitro (Daly, 1982; Pan et al., 1997; Silver et al., 2001), but no study has yet examined viscoelastic properties of human fingerpad skin in vivo.

We hypothesize that the fingerpad skin exhibits marked anisotropy, and substantial hysteretic losses under local cyclical loading, in addition to stiffening and time-dependent effects, and that these effects are significant under the large local deformations resulting from lateral traction loads. We developed an apparatus to specifically test the skin in vivo under these conditions. To evaluate elasticity, we stretched and sheared the skin with slow loading conditions. To evaluate anisotropy, we assumed the skin to be a homogeneous half-space and used this assumption to evaluate the "effective" Young's and shear moduli in specific directions, that is, the moduli of a homogenous material that would produce an equivalent behavior for a given test. It was then possible to quantitatively evaluate anisotropy as a function of ridge orientation. For viscoelasticity, we tested the skin for small deformations and identified a five-parameter model for relaxation and another for creeping. Finally, we evaluated the hysteretic loss of the skin under local cyclical loading. The skin was tested at a length scale of 0.3 mm. Saint Venant's principle allowed us to ignore deformations at distances greater than one millimeter from the region of traction. As a result, we could characterize the dermis and epidermis behaviors where most of the low-threshold receptors are located (Paré et al., 2002, 2003; Nolano et al., 2003), and minimize the influence of the global deformation of the subcutaneous tissues.

2 Methods and Materials

2.1 Subjects

Twelve right-handed subjects, nine males and three females, volunteered to participate (Table 1). Only the right index finger skin was tested. No subjects reported having a history of skin pathology. The informed consent of the subjects was obtained in accordance with the requirements of the McGill University Policy on the Ethical Conduct of Research Involving Human Subjects.

Table 1
Subjects information (mean ± standard deviation).

Protocol	Subjects		Age	Body mass	Height
	♀	♂	(years)	(kg)	(cm)
Tuning	1	1	31 ± 2	65 ± 14	167 ± 5
Elasticity	3	5	28 ± 3	68 ± 18	174 ± 15
Relaxation	3	5	29 ± 3	67 ± 18	174 ± 15
Creep	2	6	29 ± 3	70 ± 16	176 ± 12
Hysteresis	1	2	31 ± 2	58 ± 14	168 ± 3.0

Refer to Section 2.3 for a description of the protocols.

2.2 Apparatus

We designed an apparatus that could deform the skin in the large deformation range (i.e. $\sim 100\%$) and had wide operational bandwidth. With proper feedback control, it could load the skin under isotonic or under isometric conditions. Previously, we found that piezoelectric bimorph benders could stretch the skin to provide acceptable levels of sensation (Pasquero and Hayward, 2003). However, this was limited because cantilevers are too compliant. A cantilever parallel bender (Figure 1a) has this constituent equation (Smits et al., 1991):

$$\delta = g\ f^z + \delta_{\text{Free}}\, V/V_{\max}, \tag{1}$$

where δ is the tip deflection, g the compliance, f^z the force at the tip, δ_{Free} the free deflection, V the applied voltage, and $V_{\max}$ the maximum voltage, with

$$g = \frac{l^3}{2Ewh^3} \quad \text{and} \quad \delta_{\text{Free}} = \frac{3d_{31}l^2}{4h^2}V_{\max}, \tag{2}$$

where E is the piezo material's Young's modulus, l and w are the length and width of the layers, and d_{31} is the piezoelectric coefficient. The compliance varies with l^3 and the free deflection with l^2. Hence, there exists an optimal length l_{opt} that maximizes deflection for a given load. With the best commercial benders, we found that a cantilever could not deform the skin in the large range, even at l_{opt}. Now, if the benders are hinged at two places, termed "dual-pinned lever", as shown in Figure 1b, the compliance and the free deflection become (Supplementary Information):

$$g = \frac{(l_1 + l_2){l_2}^2}{2Ewh^3} \quad \text{and} \quad \delta_{\text{Free}} = \frac{3d_{31}(l_1 + l_2)l_2}{4h^2}V_{\max}. \tag{3}$$

To fabricate a cantilevered bender to achieve the same deflection as a dual-pinned bender, its length l would have to be $\sqrt{(l_1 + l_2)l_2}$. Its compliance, $[(l_1 + l_2)l_2]^{3/2}/(2Ewh^3)$, is always larger than that of the dual-pinned beam which is $[(l_1+l_2){l_2}^2]/(2Ewh^3)$. Moreover, a dual-pinned bender will always produce a higher blocked force for an equivalent deflection. By varying the ratio l_1/l_2 it is also possible to trade stiffness for free deflection.

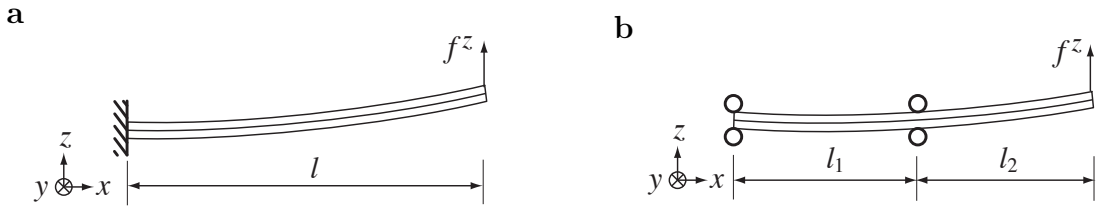

Fig. 1. **a)** Cantilered bender. **b)** Dual-pinned bender.

This was applied to the construction of the apparatus depicted in Figure 2. Two Y-poled parallel bimorph benders (Model T220-H4-303Y; Piezo Systems Inc., Cambridge, MA, USA) formed dual-pinned "tweezer". The upper pin was attached to a positioning stage (Model 4076M; Parker Hannifin Corporation, Rohnert Park, CA, USA) to vary the ratio l_1/l_2. A two-channel high voltage amplifier (Model 3584JM; Texas Instruments Inc., Dallas, TX, USA) drove the actuators. The tips

of the benders were insulated with several layers of acrylic enamel. The deflection was found by measuring the displacement of a laser beam (Model 1107/P; JDS Uniphase, San Jose, CA, USA) reflected by a mirror glued near the tip (NT32-354; Edmund Industrial Optics, Barrington, NJ, USA). Displacement was detected by a lateral position sensing device (PSD, Model DL-10; UDT Sensors, Inc., Hawthorne, CA, USA). A vertically adjustable gutter and athletic tape immobilized the subject's finger.

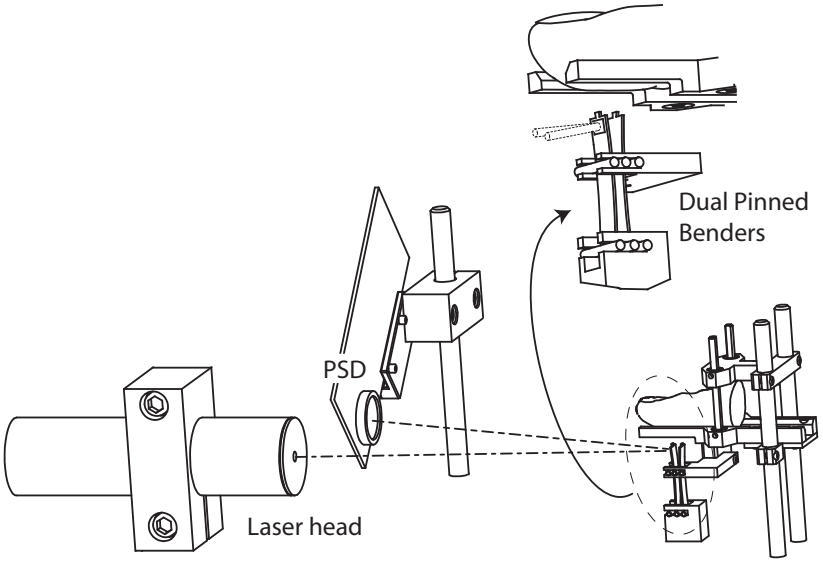

Fig. 2. Apparatus. The subject's finger was constrained in a vertically adjustable gutter that could be lowered until it touched the tips of a pair of dual-pinned piezoelectric benders. Micrometric stages made it possible to reach various places and orientations on the finger tip. Bender deflection was measured with a laser beam reflected by a small mirror attached near the tip of a bender and shinning onto a PSD detector. The piezoelectric actuators could be activated in closed loop to achieve isometric or isotonic loading.

The coefficient d_{31} was calibrated by applying a quasi-static ramping voltage signal while recording the deflection. From the slope, the coefficient was estimated (Supplementary Information). By applying a known load to the tip of the bender (15 g weight), the Young's modulus was obtained. To minimize errors, the experiments were conducted for l_2 equal to 7, 9, 11, 13, and 15 mm. The results agreed to within 5%. The errors caused by actuator hysteresis were compensated by recording the unloaded voltage-deflection relationships.

When loaded, the deflection was a solution of $\delta = cf^z(\delta, t) + \delta_{\text{Free}} V/V_{\max}$, where $f^z(\delta, t)$ is a nonlinear time-varying function. The higher the l_2/l_1, the more compliant the structure and the larger the free deflection. In order to find a tradeoff, with the help of two subjects (Table 1), l_2 was varied by 2 mm steps, and the corresponding loaded deflections were recorded. This was repeated four times with each subject. The skin was allowed to recover from viscoelastic effects for at least 30 seconds between trials. Typical force-strain curves are seen in Figure 3. When $l_2 = 11$ mm ($l = 30$ mm), the strain was maximized for both subjects. Analysis of variance (ANOVA) was performed on the maximal strains that the apparatus could create. The p-values were smaller than 0.001 when comparing deflections for $l_2 = 11$ mm with those obtained for any

other value.

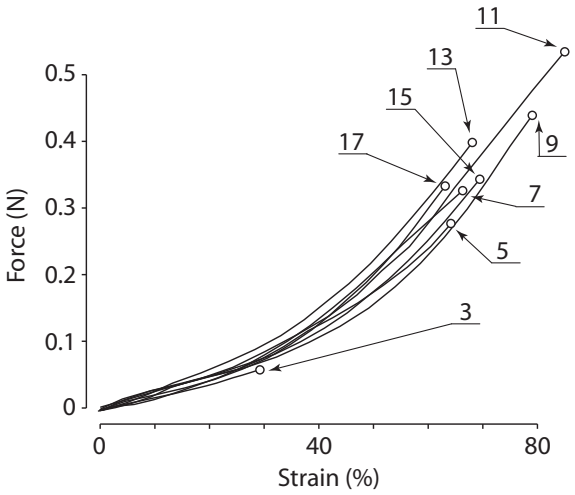

Fig. 3. Typical force-strain curves for different l_2 values. This data is for one subject. Deformation is optimized for $l_2 = 11$ mm where the skin is tangentially strained at almost 100%.

The apparatus created isometric or isotonic testing conditions by using a principle similar to the feedback modes in atomic force microscopy (Binnig et al., 1986). After calibration, the deflection δ can be written:

$$\delta = k_1 F + k_2 V. \tag{4}$$

For isotonic tests, the force $F = (\delta - k_2 V)/k_1$ was regulated by a lead dynamic compensator C_t, Figure 4a. This provided the desired amount of bending regardless of the deflection caused by a load. For isometric tests, the deflection δ was regulated using another lead compensator C_m, Figure 4b, where the unknown force F supplied by the load is a low frequency exogenous disturbance.

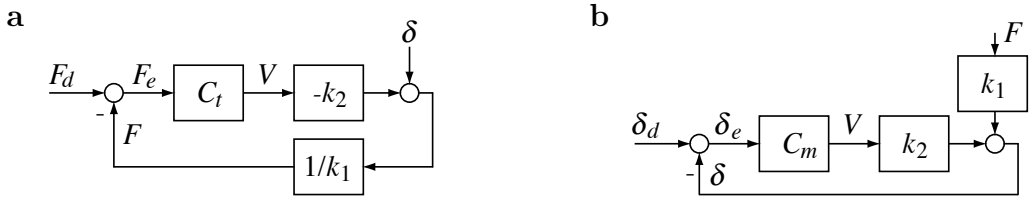

Fig. 4. **a)** Isotonic feedback. This configuration regulates the force applied by bending the actuators by the amount required to achieve a desired force. **b)** Isometric feedback. Here, the tip position is regulated regardless of the load.

2.3 Procedure

Subjects washed their hands and dried them with facial tissue before each test. A sub-millimetric area of the skin close to the papillary whorl was randomly selected. For all protocols, the tests were oriented along and across ridges. After each experiment, the tips of the benders were cleaned. Bonding was achieved by applying a thin layer of cyanoacrylate adhesive to the

tips just before lowering the finger with a micrometric stage to make contact. The height of the fingerpad was adjusted so the skin did not appear to be pulled nor indented when examined using a 10x magnifying glass. Some tips were prepared for stretch tests and some others for shear tests. Traction surfaces are shown in Figures 5a and 5b.

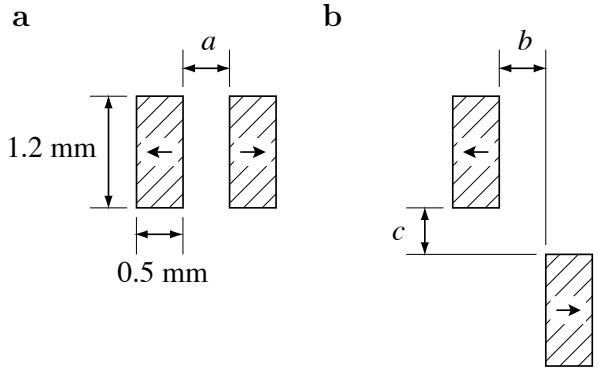

Fig. 5. Traction areas. The initial distances a and b were determined by the initial voltage applied to the actuators for a given test. **a)** Stretch tests. **b)** Shear tests.

Skin elasticity in tangential traction. Elasticity was examined both by stretching and shearing the skin. For stretching, the initial distance a between the traction surfaces was 0.25 mm. For shearing, b was 0.25 mm and c was 1.0 mm.

Relaxation testing. Patches of skin ($a = 0.4$ mm) were subjected to a pseudo-random lateral displacement signal switching from 0.015 mm to 0.06 mm applied tangentially at an average frequency of 0.2 Hz under isometric conditions. The skin behaved linearly in this range.

Creep testing. Patches of skin ($a = 0.3$ mm) were stretch-loaded isotonically using a pseudo-random force signal. The signal had frequencies centered around 0.8 Hz and its amplitudes switched from 0.025 N to 0.25 N. The skin behaved linearly in this range.

Hysteresis testing. Patches of skin ($a = 0.3$ mm) were stretched cyclically. The driving voltages were ramped at a constant rate from -80 V to +80 V, and back to -80 V. Unloading began immediately after loading and four different rates were used, yielding cycles of 10, 20, 40, and 80 seconds.

2.4 Data processing

All data were analyzed using Matlab™ (The Math Works Inc., Natick, MA, USA) along with its system identification and statistics toolboxes.

Effective Young's and Shear modulus. For a homogenous isotropic half-space, the deformation displacement function of Boussinesq and Cerruti caused by a distributed tangential force along

the x axis is (Johnson, 1985):

$$u_x = \frac{1}{4\pi G}\iint_S q_x(\xi,\eta)\left(\frac{1}{\rho}+\frac{1-2\upsilon}{\rho+z}+\frac{(\xi-x)^2}{\rho^3}-\frac{(1-2\upsilon)(\xi-x)^2}{\rho(\rho-z)^2}\right)d\xi d\eta \tag{5}$$

where u_x is the displacement, $\rho = \sqrt{(\xi-x)^2+(\eta-y)^2+z^2}$, S is the loading area, $q_x(\xi,\eta)$ is the distribution of the tangential force, υ and G are the Poisson's ratio and shear modulus of the skin respectively. The Poisson ratio for soft tissues can be taken to be 0.5. In addition, the tangential force distribution in the bonded area could be assumed to be uniform. The above expression simplifies to

$$u_x = \frac{f_T}{4\pi GA}\iint_S\left(\frac{1}{\rho}+\frac{(\xi-x)^2}{\rho^3}\right)d\xi d\eta = \frac{f_T}{4\pi GA}\Psi(x), \tag{6}$$

where f_T is the tangential load and A the traction area. The value of $\Psi(x)$ was evaluated for the traction areas in Figure 5 and the effective value of $E = 2(1+\nu)G = 3G$ obtained from both stretch and shearing tests.

Relaxation and Creep Functions. Following Radok's suggestion as in (Johnson, 1985), the displacement along x axis is:

$$u_x(t) = \int_0^t c(t-\tau)\frac{d\frac{f_T(\tau)}{4\pi GA}\Psi(x)}{d\tau}d\tau = \frac{\Psi(x)}{4\pi GA}\int_0^t c(t-\tau)\frac{df_T(\tau)}{d\tau}d\tau, \tag{7}$$

Since the system is causal, applying the Laplace transform yields

$$\begin{aligned} L[u_x(t)] = U_x(s) &= \frac{\Psi(x)}{4\pi GA}\int_0^\infty\left[\int_0^\infty c(t-\tau)\frac{dF_T(\tau)}{d\tau}d\tau\right]e^{-st}dt \\ &= \frac{\Psi(x)}{4\pi GA}\int_0^\infty\frac{dF_T(\tau)}{d\tau}e^{-s\tau}d\tau\int_0^\infty c(t)e^{-st}dt \\ &= \frac{\Psi(x)}{4\pi GA}sF_T(s)C(s) \end{aligned} \tag{8}$$

Modeling the response as that of a viscoelastic solid represented by a model as in Figure 6, the transfer function from input displacement u to output force f_T is found to be:

$$f_T = \mu_0 u + \mu_1 u_1 + \mu_2 u_2, \qquad f_T = \mu_0 u + \eta_1\dot{u}_1 + \eta_2\dot{u}_2. \tag{9}$$

After calculations,

$$\frac{F_T(s)}{u(s)} = R(s) = \frac{1}{C(s)} = \mu_0 + \frac{\eta_1\mu_1 s}{\mu_1+\eta_1 s} + \frac{\eta_2\mu_2 s}{\mu_2+\eta_2 s} \tag{10}$$

For a more compact form, let $E_R = \mu_0$, $\tau_1 = \frac{\eta_1}{\mu_1}$, $\sigma_1 = \frac{\eta_1}{\mu_0}(1+\frac{\mu_0}{\mu_1})$, $\tau_2 = \frac{\eta_2}{\mu_2}$, and $\sigma_2 = \frac{\eta_2}{\mu_0}(1+\frac{\mu_0}{\mu_2})$. The relaxation function $R(s)$ and the creep function $C(s)$ then are:

$$R(s) = \frac{1}{C(s)} = \frac{E_R+(\sigma_1+\sigma_2)s+(\sigma_1\tau_2+\sigma_2\tau_1-E_R\tau_1\tau_2)s^2}{(1+\tau_1 s)(1+\tau_2 s)}. \tag{11}$$

Using the bilinear transformation $s = \frac{2}{T}(z-1)/(z+1)$ to substitue s, we obtained a discrete-time domain transfer function that could be identified using an ARMAX procedure.

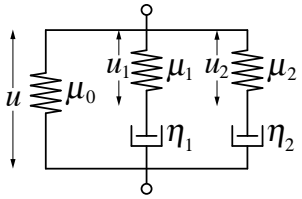

Fig. 6. Second order linear viscoelastic material model. This model yielded a much better fit than a first order viscoelastic model due to the presence of two relaxation rates.

3 Results

3.1 Young's modulus

A typical nonlinear skin force-strain curve is seen in the Figure 7. Because of the tangential traction, there was no clearly defined "knee" in the curve although the skin became very stiff beyond 50% strain. The means and standard deviations of the Young's modulus are collected in Figure 8 for all eight subjects. The moduli found by stretching the skin along ridges were consistently higher than those found by stretching it across ridges. In Figure 8 the results are sorted by order of decreasing differences between directions. For each subject, a two-sample, two-tailed Student t-tests was conducted on the Young's moduli found by stretching and shearing along and across ridges which all rejected the null hypothesis (5% significance level).

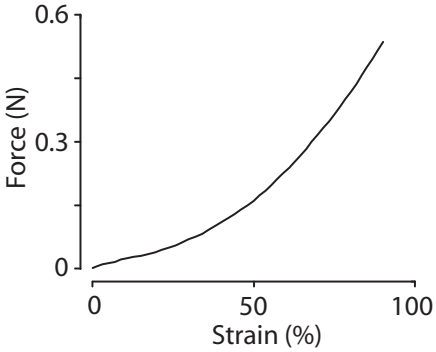

Fig. 7. Nonlinear force-strain relationship of the skin of one subject.

ANOVA was used to compare the mean Young's modulus found by stretching/shearing the skin along ridges with that across ridges, see Table 2. The Young's moduli were significantly dependent on the direction of the deformation relative to the orientation of the ridges ($p = 0.012$ and $p = 0.023$ for the stretching and the shearing conditions respectively). In both conditions, the skin was stiffer along the ridges than across them. Conversely, ANOVA tests yielded no significant difference between two groups of Young's moduli measured along proximal-distal direction versus

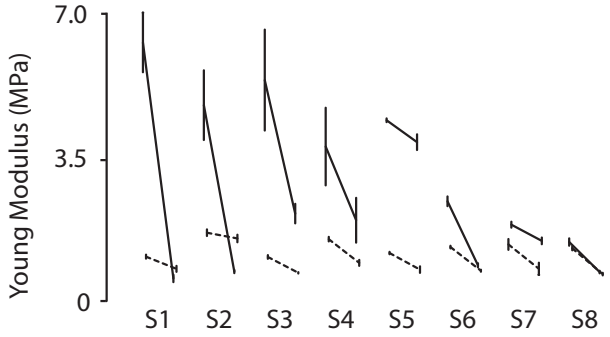

Fig. 8. Skin moduli of eight subjects listed on the horizontal axis. Solid line shows the effective Young's moduli measured by stretching the skin, and the dashed line by shearing the skin. For each subject, left: effective Young's moduli of the skin along the ridges; right: across the ridges. For some subjects, the moduli found by stretching traction is highly dependent on the ridge orientation but less for others (solid lines). The moduli found by shearing are less sensitive to ridge orientation, yet consistently different (dashed lines).

the radial-ulnar direction ($p = 0.474$ for the stretching condition, and $p = 0.675$ for the shearing condition), implying that the stiffness difference was related to the direction of ridge, but not to the orientation of the test with respect to the finger.

Table 2
Mean ± standard deviation skin moduli for all eight subjects.

	Along ridges (MPa)	Across ridges (MPa)
Stretching	3.61 ± 1.73	1.54 ± 1.08
Shearing	1.36 ± 0.27	0.96 ± 0.34

3.2 Relaxation

Figure 9 shows typical relaxation when the skin is subjected to a pseudo-random isometric test. The uniaxial force decreased rapidly over the first 5-8 seconds, then the relaxation rate was low until the force reached a steady value. This justified the choice of a model having one elastic term and two time constants. The five parameters of the linear standard solid were identified for each subject and listed in Table 3. ANOVA tests found no significant differences along and across ridges.

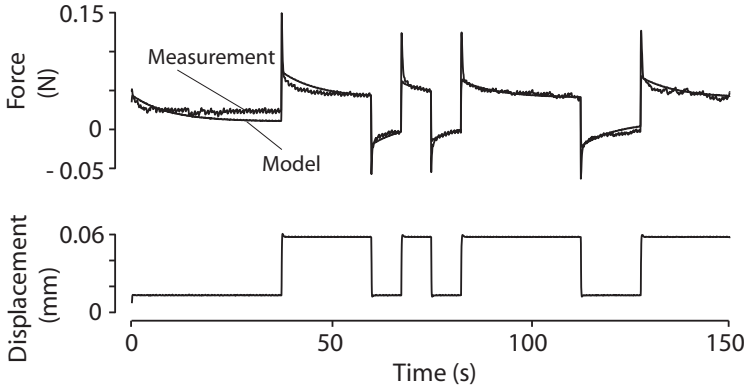

Fig. 9. Relaxation behavior of the skin. For many subjects, after each displacement transient, the force dropped abruptly and then slowly relaxed over a long time period.

Table 3
Relaxation protocol parameter fit for all eight subjects.

	Along						Across					
	μ_0	μ_1	η_1	μ_2	η_2	r^2fit	μ_0	μ_1	η_1	μ_2	η_2	r^2 fit
S1	0.69	0.44	0.18	0.63	0.001	81%	0.93	0.85	0.06	1.95	0.002	78%
S2	0.54	0.62	0.24	5.18	0.053	81%	0.35	0.18	0.36	0.37	0.001	82%
S3	1.26	0.70	0.52	8.55	0.044	55%	0.85	1.48	0.89	9.76	0.113	50%
S4	0.87	0.91	1.12	17.79	0.095	64%	0.49	0.88	1.43	13.36	0.089	76%
S5	2.97	0.56	1.85	0.88	0.022	82%	0.93	0.90	0.40	2.52	0.124	86%
S6	0.92	1.26	0.83	4.92	0.169	78%	1.01	1.73	1.16	4.07	0.145	79%
S7	0.43	1.07	0.40	10.81	0.084	88%	0.60	0.32	0.50	6.13	0.085	93%
S8	0.72	0.40	0.31	9.38	0.064	83%	0.99	0.30	1.60	8.09	0.051	86%

All eight subjects were tested. Much variability across subjects was observed.

3.3 Creep

Figure 10 shows a typical creep curve when the skin is subjected to a pseudo-random isotonic test. When stretched by a constant force, the skin elongated at high rate. The deformation decreased slower than it increased, implying that hysteresis existed. A fit for the five parameters of the linear standard solid was attempted for each subject. These are listed in Table 4. ANOVA failed to find significant differences among tests along and across ridges.

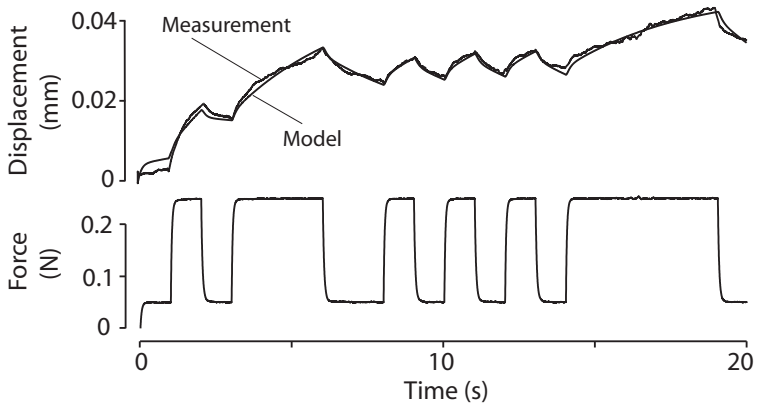

Fig. 10. Creeping behavior of the skin. Force transients caused the skin to creep about twice slower than it relaxed. Visual inspection and comparison can be misleading.

Table 4
Creep protocol parameter fit for all eight subjects.

	Along						Across					
	μ_0	μ_1	η_1	μ_2	η_2	r^2fit	μ_0	μ_1	η_1	μ_2	η_2	r^2fit
S1	2.20	7.92	1.10	15.09	0.40	93%	0.41	4.99	1.67	11.34	0.51	90%
S2	1.62	1.37	2.38	37.65	1.86	83%	0.17	1.82	3.92	42.65	1.19	81%
S3	0.71	7.15	2.46	10.84	0.18	89%	0.75	2.88	3.68	43.53	2.76	79%
S4	0.04	1.69	16.44	19.83	2.60	78%	0.23	1.31	32.04	13.76	2.83	86%
S5	0.14	0.48	1.28	2.75	0.48	76%	0.34	4.15	54.96	6.59	2.92	76%
S6	0.11	0.48	1.19	1.40	0.55	93%	0.20	0.89	1.63	1.44	0.25	91%
S7	1.42	6.38	2.86	15.14	0.33	84%	0.06	2.54	18.84	31.18	2.54	80%
S8	1.09	4.13	4.74	33.86	1.18	86%	0.99	6.55	2.23	19.33	1.13	85%

All eight subjects were tested. Much variability across subjects was observed.

3.4 Hysteresis

The skin of all three subjects exhibited strong hysteresis with substantial energy loss (81.1% on average). Typical hystereses for one subject are shown in Figure 11 for various loading and unloading times. The responses are highly repeatable and essentially invariant for times longer than 20 seconds. It is only with faster stimulation (5 second loading and 5 second unloading) that the losses tended to diminish. ANOVA found no significant effects of the ridge orientation ($p = 0.672$), and no significant effect of the loading and unloading time, once large enough ($p = 0.826$).